













# Linear Regression vs. Deep Learning for Signal Quality Monitoring in Coherent Optical Systems

Yuchuan Fan , *Graduate Student Member, IEEE*, Xiaodan Pang , *Senior Member, IEEE*, Aleksejs Udalcovs , *Senior Member, IEEE*, Carlos Natalino , *Member, IEEE*, Lu Zhang , *Member, IEEE*, Sandis Spolitis , *Member, IEEE*, Vjaceslavs Bobrovs , *Member, IEEE*, Richard Schatz , Xianbin Yu , *Senior Member, IEEE*, Marija Furdek , *Senior Member, IEEE*, Sergei Popov , and Oskars Ozolins , *Senior Member, IEEE*

**Abstract**—Error vector magnitude (EVM) is a metric for assessing the quality of m-ary quadrature amplitude modulation (mQAM) signals. Recently proposed deep learning techniques, e.g., feedforward neural networks (FFNNs) -based EVM estimation scheme leverage fast signal quality monitoring in coherent optical communication systems. Such a scheme estimates EVM from amplitude histograms (AHs) of short signal sequences captured before carrier phase recovery (CPR). In this work, we explore further complexity reduction by proposing a simple linear regression (LR) -based EVM monitoring method. We systematically compare the performance of the proposed method with the FFNN-based scheme and demonstrate its capability to infer EVM from an AH when the modulation format information is known in advance. We perform both simulation and experiment to show that the LR-based EVM estimation method achieves a comparable accuracy as the FFNN-based scheme. The technique can be embedded with modulation format identification modules to provide comprehensive

signal information. Therefore, this work paves the way to design a fast-learning scheme with parsimony as a future intelligent OPM enabler.

**Index Terms**—Deep learning, error vector magnitude, machine learning, optical fiber communication, optical performance monitoring.

## I. INTRODUCTION

THE introduction of bandwidth-consuming services, such as cloud computing, 5G networks, and virtual reality (VR), bring the continuously increasing demands for data. Optical networks as the backbone infrastructure of carrying these applications are pressured to become more heterogeneous and dynamic to support the exponential growth of data traffic. Coherent transceiver technologies along with high order modulation formats are widely employed for transmission links beyond 100 Gbit/s data rate per wavelength [1]. Moreover, the reconfigurable dynamic networks, such as elastic optical networks (EONs), are a means to improve network capacity and scalability [2]. It can dynamically adjust network configurations e.g., modulation formats, data rate, spectrum planning, according to different channel conditions to increase the utilization efficiency of bandwidth resources [3]. However, these enhanced features will lead to the increased complexity of manipulating available resources for heterogeneous vendors and technical domains [4]. Consequently, it is necessary to implement a comprehensive and intelligent optical performance monitoring (OPM) system to ensure effective network management and diagnose faults [3]–[6]. There are generally two types of OPM that gained considerable attention in research: OPM at intermediate network nodes and OPM at end nodes [7]–[10]. At the intermediate nodes, reconfigurable optical add/drop multiplexers (ROADMs) are often employed to amplify and switch the incoming optical signals, where inline OPM modules can be placed to monitor the optical signal quality of the channels. Commonly monitored metrics are signal power, chromatic dispersion (CD), and optical signal to noise ratio (OSNR). At the end nodes, the data information will be recovered, and the monitoring functionality normally is a configured by the digital signal processing (DSP) algorithms in the digital coherent optical (DCO) transceivers. In both cases, accurate telemetry of key performance indicators such as bit error rate (BER) can extend monitoring functionality

Manuscript received 9 June 2022; revised 11 July 2022; accepted 21 July 2022. Date of publication 25 July 2022; date of current version 3 August 2022. This work was supported in part by the China Scholarship Council under Grant 201807930003, in part by the Swedish Research Council projects under Grants 2019-05197 and 2016-04510, in part by the RISE SK funded project Optical Neural Networks under Grant P109599, in part by the ERDF-through the CARAT Project under Grant 1.1.1.2/VIAA/4/20/660, in part by the National Key Research and Development Program of China under Grant 2018YFB2201700, and in part by the VINNOVA through the CELTIC-NEXT Project AI-NET PROTECT under Grant 2020-03506. (*Corresponding author: Oskars Ozolins.*)

Yuchuan Fan and Xiaodan Pang are with the Applied Physics Department, KTH Royal Institute of Technology, 106 91 Stockholm, Sweden, and also with the RISE Research Institutes of Sweden, 164 40 Kista, Sweden (e-mail: yuchuanf@kth.se; xiaodan@kth.se).

Aleksejs Udalcovs is with the RISE Research Institutes of Sweden, 164 40 Kista, Sweden (e-mail: aleksejs.udalcovs@gmail.com).

Carlos Natalino and Marija Furdek are with the Electrical Engineering Department, Chalmers University of Technology, 412 96 Gothenburg, Sweden (e-mail: carlos.natalino@chalmers.se; furdek@chalmers.se).

Lu Zhang and Xianbin Yu are with the College of Information Science and Electronic Engineering, Zhejiang University, Hangzhou 310027, China, and also with Zhejiang Lab, Hangzhou 310000, China (e-mail: zhanglu1993@zju.edu.cn; xyu@zju.edu.cn).

Sandis Spolitis and Vjaceslavs Bobrovs are with the Institute of Telecommunications, Riga Technical University, 1048 Riga, Latvia (e-mail: sandis.spolitis@rtu.lv; vjaceslavs.bobrovs@rtu.lv).

Richard Schatz and Sergei Popov are with the Applied Physics Department, KTH Royal Institute of Technology, 106 91 Stockholm, Sweden (e-mail: rschatz@kth.se; sergeip@kth.se).

Oskars Ozolins is with the Applied Physics Department, KTH Royal Institute of Technology, 106 91 Stockholm, Sweden, with the RISE Research Institutes of Sweden, 164 40 Kista, Sweden, and also with the Institute of Telecommunications, Riga Technical University, 1048 Riga, Latvia (e-mail: oskars.ozolins@ri.se).

Digital Object Identifier 10.1109/JPHOT.2022.3193727

and are prerequisites for signal quality assessment [11], [12]. Error vector magnitude (EVM) is an alternative signal quality characterization metric in the case of complex modulation formats, such as m-ary quadrature amplitude modulation (mQAM) [13], [14]. Traditionally, the EVM calculation requires the collection and processing of millions of received symbols using the full stack of DSP routines. This accumulative process is quite time-consuming and not suitable for monitoring dynamic optical networks.

The existing methods rely on statistical analysis, for instance, on the fourth-order moments or cumulative distribution function of the received signal for OPM [15], [16]. At the same time, deep learning has regained popularity in the optical communication community, where classical deep learning applications include OPM, equalization, quality of transmission estimation, etc [3], [17], [18], which shows promising and versatile performance. Recently, we proposed deep learning-based EVM estimation schemes from a short signal sequence for fast signal quality monitoring in coherent optical systems [19]–[21]. We have demonstrated accurate and effective EVM estimators by constructing deep learning-based regressor from constellation diagrams [19] and amplitude histograms (AHs) [20]. In [19], we proposed a CNN based EVM estimator to extract features from the image dataset of the constellation diagram. Later, an FFNN powered EVM estimation scheme was implemented for AHs before the carrier phase recovery (CPR) module [20]. Thanks to the direct operation on the AH vectors, the FFNN can further reduce the model complexity used for EVM estimation. Compared with the CNN scheme, FFNN relaxes not only DSP requirements but also energy consumption in the EVM estimation process itself. Moreover, the robustness of the FFNN-based EVM estimator for systems with laser phase noise was demonstrated in [21]. Although the deep learning-based regressors have shown promising capability of estimating EVM, one may still argue that a parsimonious model might be also competent for this work under certain circumstances. One typical example is the linear regression (LR), which is the fundamental component of the deep learning-based regressor, and can be viewed as an FFNN model without hidden layers and nonlinear activation functions [22]. In [23], we have reported that the LR can be implemented for EVM estimation in certain cases.

In this paper, we thoroughly investigate the LR-based EVM estimator performance in coherent optical systems. The LR-based estimator is implemented on AHs obtained from short mQAM sequences captured before the CPR module in coherent transceivers. In addition, we include the FFNN-based EVM estimation scheme as a benchmark [20]. Unfortunately, the LR algorithm has limited capability to partition data in hyperspace unlike deep learning models using hidden layers and nonlinear activation functions to be the universal function approximators [24]. We firstly benchmark the performance of the LR-based EVM estimator with the optical back-to-back (OB2B) configuration. In this scenario, we collect datasets of quadrature phase-shift keying (QPSK), 16QAM, 64QAM signals across wide OSNR ranges. The LR model is implemented for each modulation format separately. Secondly, we collect datasets with a long-haul transmission simulation setup containing QPSK, 16QAM, 64QAM signals transmitted over 2000-, 1500-,

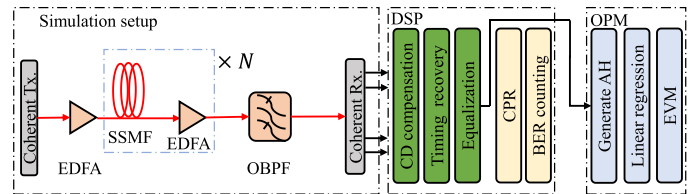


Fig. 1. Schematic diagram of the proposed EVM estimation scheme and long-haul transmission setup. EDFA, erbium-doped fiber amplifier; SSMF, standard single-mode fiber; OBPF, optical bandpass filter; DSP, digital signal processing; CD, chromatic dispersion; CPR, carrier phase recovery.

1000-km fiber links, respectively. Using these datasets, we test the generalization capability of the LR scheme, i.e., training a different number of modulation formats in one LR model. Lastly, the generalization of the LR scheme is investigated on a wavelength-division multiplexed (WDM) transmission system. Besides, experimental validation is conducted by a 28 Gbaud setup with square 64QAM (sq-64QAM) and circular 64QAM (c-64QAM) signals. The results show that the LR-based estimator achieves comparable performance with the FFNN scheme when we train each modulation format separately. This indicates that a simple LR-based regressor can enable the EVM estimation functionality for an intelligent OPM module, by combining it with the modulation formats identification (MFI) function of OPM. One should note that this work focuses on constellations of uniformly distributed symbols. Owing to their specific properties, estimating EVM and quantifying the link between EVM and BER for the probabilistic-shaped modulation formats should be covered with a dedicated separate study.

## II. PRINCIPLES

### A. Simulation Dataset Collection

To collect the AH datasets, we build a 32 Gbaud coherent transmission setup in VPItransmissionMaker [25] as shown in Fig. 1. At the coherent transmitter's side, the generated pseudorandom bit sequence of  $2^{15}-1$  word-length (PRBS15) is firstly repeated and only then mapped into mQAM symbols. The Nyquist pulse filter shapes the mQAM symbols to bandwidth-limited electrical signals, where the root-raised cosine filter has a 0.15 roll-off factor. Then, a Mach-Zehnder-based in-phase and quadrature modulator (IQM) is applied to convert the electrical signals to optical signals at a laser central wavelength of 1550 nm. The optical signals are amplified by an erbium-doped fiber amplifier (EDFA) and transmitted through the multiple fiber spans long-haul transmission link. Each span contains a 100 km long standard single-mode fiber (SSMF) and an inline EDFA. We configure the SSMF parameters with a  $16\text{e-}6$  s/m<sup>2</sup> chromatic dispersion (CD) coefficient, a 0.2 dB/km attenuation coefficient, and a  $2.6\text{e-}20$  m<sup>2</sup>/W nonlinear refractive index. The launch power is optimized to ensure the transmission system is operated in the linear region. We set 45 dB initial OSNR before the transmission and measure the OSNR at 0.1 nm resolution after a set of transmission spans by using an optical spectrum analyzer. The maximum transmission distance is 2000 km, 1500 km, and 1000 km for QPSK, 16QAM, and 64QAM, respectively. The received signals are coherently detected and saved for offline

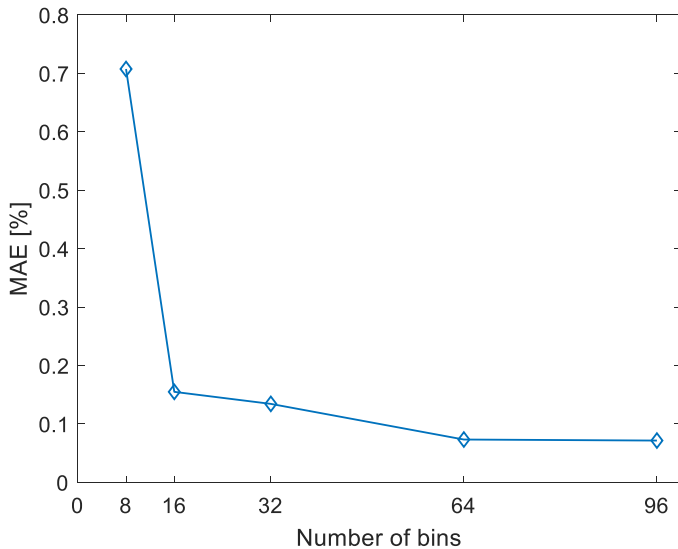


Fig. 2. The FFNN-based estimator performance versus different number of bins on the 6400-symbol dataset.

digital signal processing (DSP) and generating AH datasets. After a full DSP routine, we collect and measure EVM labels by the mean-square (rms) value of the difference between ideal (reference) transmitted symbols and the received symbols [13], [14]. The reference transmitted symbols are obtained using the K-means clustering method [19].

We choose the length of the signal sequence containing symbols from 100 to 6400 to study the estimation performance, where the 6400 is an acceptable number of symbols for 64QAM reported in [20]. Besides, signal sequences are captured before a CPR module in the DSP. An AH of a signal sequence is generated by sorting magnitude elements of complex symbols into equally spaced bins along the x-axis between maximum and minimum values. A number of bins affects the estimation accuracy. Fig. 2 shows the performance of the FFNN-based EVM estimator for different numbers of bins. The larger number of bins, the longer signal sequence must be used to generate a good informative AH, otherwise, it affects estimation accuracy. Besides, a larger number of bins increases computational complexity of the EVM estimator. Hence, there is a tradeoff between the performance and accuracy. Considering the tradeoff, we set the number of bins to 64. The amplitude of the histogram indicates number of elements in the bin. Fig. 3 visualizes the collected 64-bin vectorized AH dataset examples, which are generated by a 6400-symbol long signal sequence. For each transmission scenario (6 transmission distance  $\times$  3 modulation formats), we collect 100 AHs and divide the dataset as 50%, 25%, 25% for training, validation, and testing.

### B. LR-Based EVM Estimator

Consider a set of  $n$  training AH vectors and corresponding EVM labels,  $\{x_i, y_i\}, i = 1, 2, \dots, n$ , the goal of LR is to learn a mapping function  $y = f(x)$ . One AH sample  $\mathbf{x} = [x_1, x_2, \dots, x_{64}]$  contains 64 explanatory variables. An LR model between  $n$  rows of AH vectors  $\mathbf{X}$  and EVM labels  $\mathbf{Y}$  can be formulated as

$$\mathbf{Y} = \mathbf{X}\beta + \varepsilon, \quad (1)$$

where  $\beta$  is the regression coefficient and  $\varepsilon$  is an error term. In our implementation, we use shuffled random seed numbers for both the bit sequence pattern and all the noise realizations in different parts of the system. Consequently, as the independently and identically distributed (i.i.d.) random symbols are experienced in an additive white Gaussian noise-dominated channel, the constructed AH vectors are i.i.d. According to the Gauss-Markov Theorem, we assume that errors of linear regression have a zero mean, homoscedasticity and uncorrelation [26]. The learned model is obtained by solving:

$$f(\beta) = \arg \min (\mathbf{Y} - \mathbf{X}\beta)^T (\mathbf{Y} - \mathbf{X}\beta). \quad (2)$$

A classic FFNN model has linear connections and nonlinear activation functions densely interconnected between input and output layers. Compared with an FFNN model, the LR-based EVM estimator has a more compact structure but limited estimation capability. Therefore, we need to design the LR-based EVM estimator in a hierarchical manner to eliminate some impacts of certain factors, such as cooperating with the MFI module. The MFI module can help to select a proper pre-trained LR model monitoring EVM for the identified modulation format. In this sense, better performance of LR is credited to the lightened task, which trains a single model for each modulation format. Besides, we also investigate a single LR model EVM estimation accuracy for multiple modulation formats.

## III. SIMULATION RESULTS

### A. Optical Back-to-Back Transmission

Before looking on the LR scheme performance with fiber transmission, we perform a study on the LR scheme for a 32 GBaud optical back-to-back (OB2B) system. In this study, we collect AH datasets of 30 transmission scenarios containing QPSK, 16QAM, and 64QAM signals. Each AH is generated by a 6400 long signal sequence captured before CPR. The OSNR values are ranged from 12 to 30 dB, 20 to 38 dB, 26 to 44 dB for QPSK, 16QAM, and 64QAM, respectively. The associated measured EVMs are 30.64 to 4.48%, 9.24 to 2.07%, 4.28 to 1.59%. These OSNR ranges ensure the BER below the hard-decision forward error correction (HD-FEC) threshold for QPSK signals, and below the soft-decision FEC (SD-FEC) threshold for 16QAM and 64QAM signals. Due to the limited estimation capability, we firstly test the estimation performance when the LR model trained for each modulation format separately. The EVM estimation results of the LR scheme are shown in Fig. 4. Fig. 4(a) illustrates mean absolute errors (MAEs) versus OSNRs for the considered modulation formats. The MAE below 0.3%, 0.1%, and 0.1% are achieved for QPSK, 16QAM, and 64QAM, respectively. It is noticed that there are MAE performance gaps between different modulation formats at some OSNRs. This is due to different EVM true labels at this OSNR point. When comparing the relative errors (aka normalized MAEs), the LR-based estimator gives more or less similar performance. Fig. 4(b) shows the distribution of EVM estimation errors using violin plots, where wider parts of the violin are attributed to a high probability and the skinnier parts indicate a low probability. Besides, the maximum, median, and minimum values are represented by its upper, middle, and lower

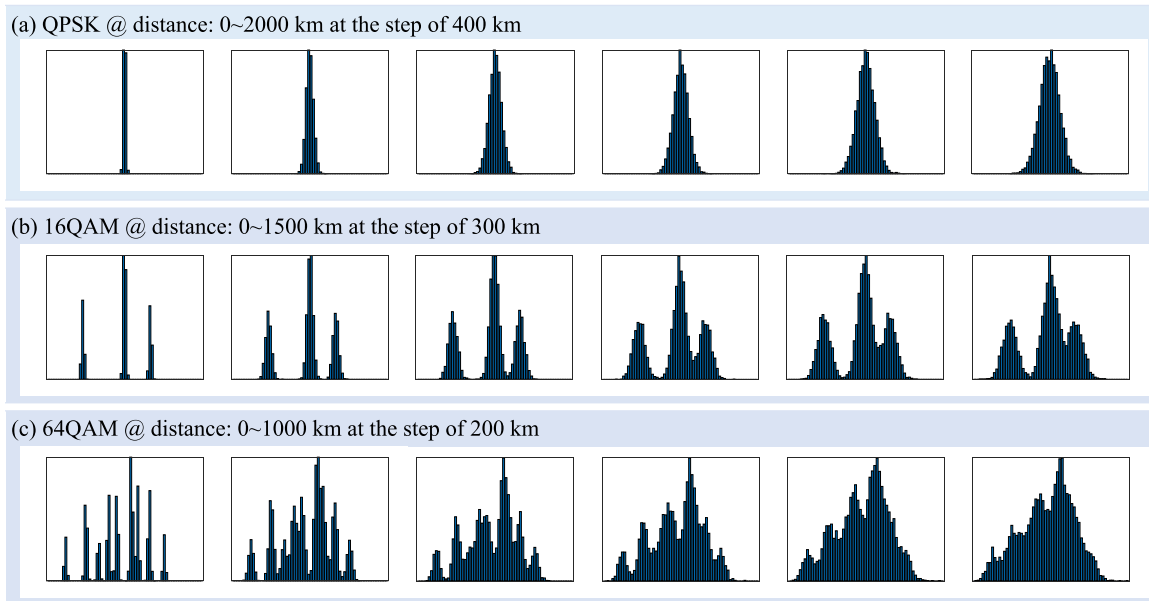


Fig. 3. The collected AH dataset examples.

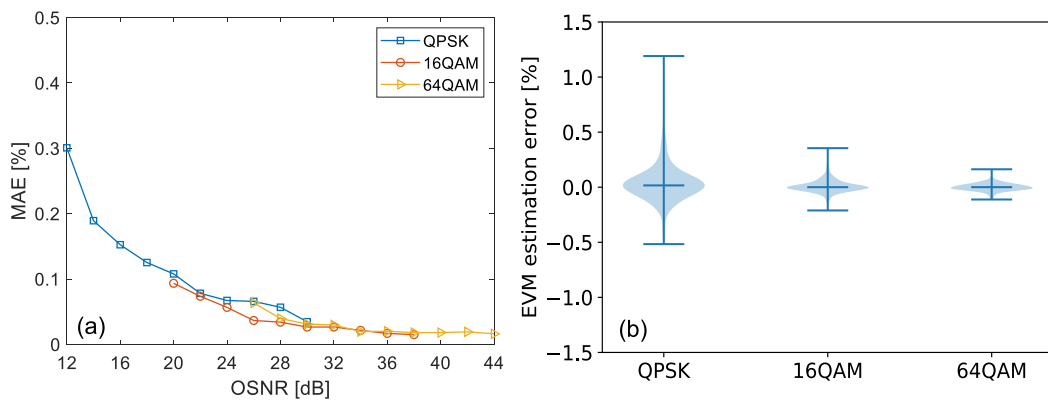


Fig. 4. The EVM estimation performance of LR scheme for OB2B transmission on test dataset, (a) MAE versus OSNR, (b) Distribution of estimation error.

bars. In this figure, each violin shape represents the distribution obtained from 250 test samples. The wider parts of violin shapes for 16QAM and 64QAM are concentrated around the median error, which shows a decent estimation performance. Although the maximum EVM estimation error for QPSK is over 1%, these outliers come from low quality of signals where the constellation clusters start to cross each other, yet the most of test samples are within 0.5%. If training each modulation format separately, the LR scheme shows a good generalization when signals operating at a wider OSNR range.

### B. Long-Haul Transmission

First, we investigate the impact of a different number of symbols and training schemes on the EVM estimation accuracy. In the training phase, we include different training methods for LR scheme to study the generalization capability: 1) LR1, training a model for each modulation format; 2) LR2, training a model with two modulation formats, here we consider 16QAM and 64QAM; 3) LR3, training a single model for three modulation

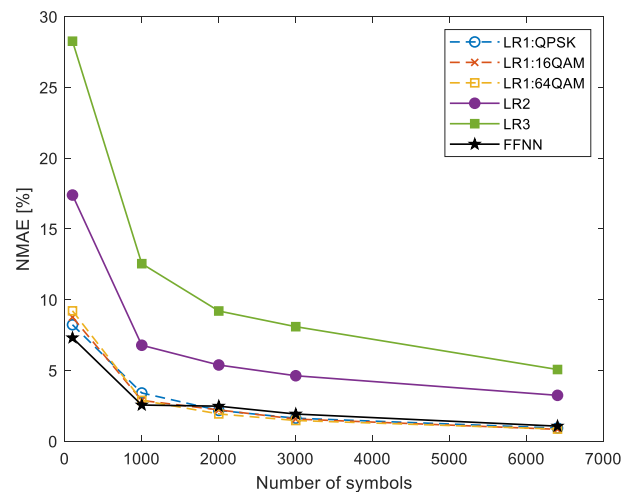


Fig. 5. Normalized mean absolute error (NMAE) of EVM estimation vs. number of symbols for various schemes of training one model. LR1: One modulation format; LR2: Two modulation formats; LR3: Three modulation formats; FFNN: Three modulation formats.

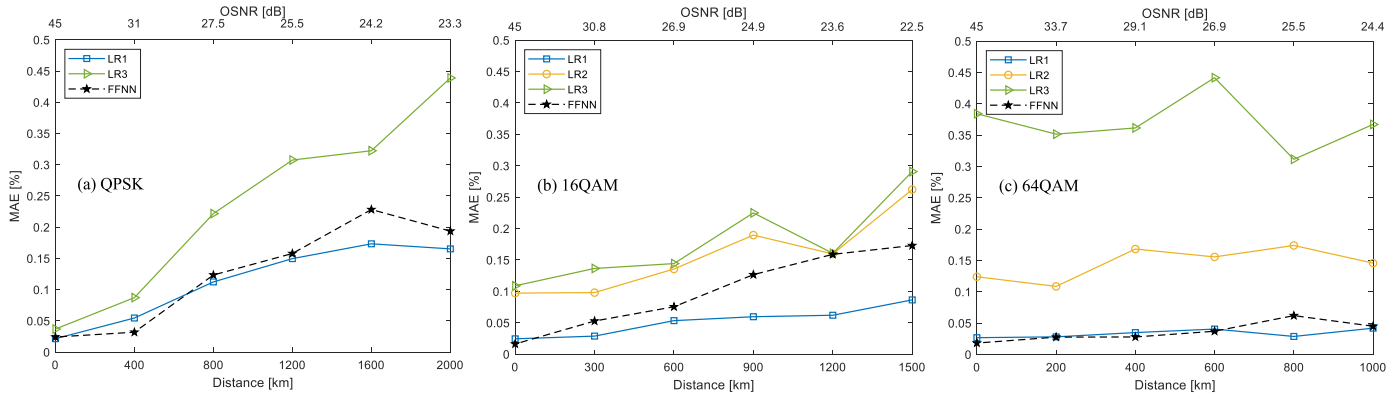


Fig. 6. Mean absolute error (MAE) of the estimated EVM values vs. different fiber transmission distances for the 6400-symbol dataset.

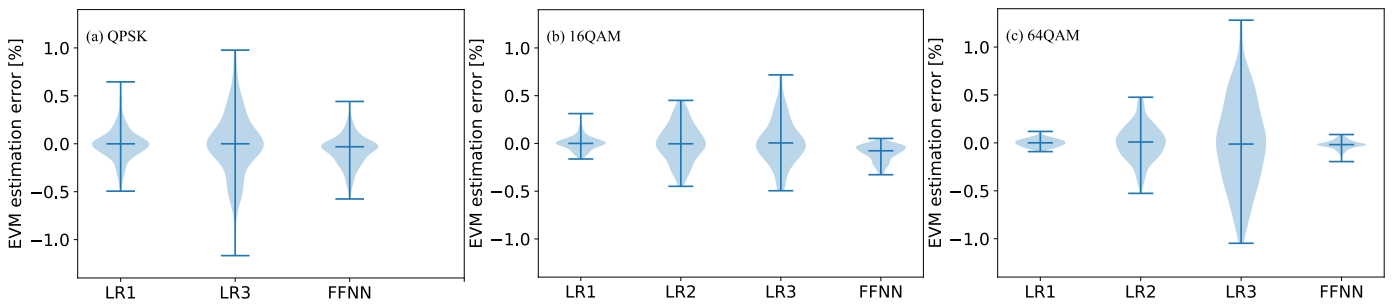


Fig. 7. Distribution of EVM estimation errors under different training scheme for 6400-symbol dataset.

formats. The employed FFNN model structure contains four hidden layers (1000, 500, 500, 100 neurons) [20], which trains a single model with all modulation formats as the reference benchmark. Fig. 5 illustrates normalized mean absolute error (NMAE) as a function of the number of symbols for different training methods. We use NMAE to evaluate accuracy across different models, which is defined as:

$$NMAE[\%] = \frac{1}{n} \sum_{i=1}^n \frac{|EVMt_i - EVMe_i|}{EVMt_i} \times 100, \quad (3)$$

where  $n$  is the number of test samples in a model,  $EVMt_i$  and  $EVMe_i$  denote  $i$ th test sample true EVM and estimated EVM, respectively. The FFNN-based EVM estimator shows a good generalization when we train all modulation formats in one model. It can be observed that there is a performance gap between curves of LR1, LR2, and LR3 models. This tendency is expected to be enlarged when more modulation formats are simultaneously included in the model. When we train an LR model for each modulation format separately, the LR scheme achieves performance as well as the FFNN scheme. For a 1000-symbol and a 6400-symbol long signal sequence, the LR1 model achieves NMAE below 3.5% and 1%, respectively.

Next, we elaborate on detailed performance for each considered modulation format, including MAEs and error deviation between true EVM labels and estimated EVM values. Here, we use a relatively long signal sequence, e.g., 6400-symbol dataset, as the test dataset. In Fig. 6 we illustrate estimated MAEs as a

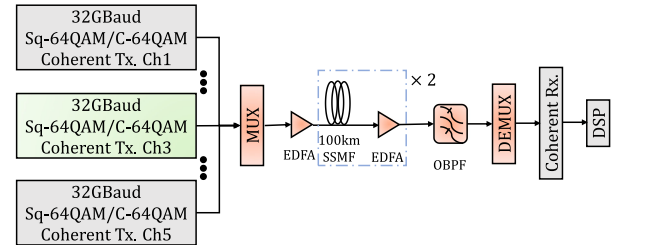


Fig. 8. Schematic diagram of simulation setup for fiber nonlinearity dataset. MUX: Multiplexer; DEMUX: Demultiplexer.

function of transmission distance. The top axis is the corresponding measured OSNR. The MAEs of LR1 for QPSK, 16QAM, 64QAM are below 0.23%, 0.16%, 0.06% respectively. As the number of modulation formats increases, the generalization capability of the LR model decreases as expected. For instance, the LR3 results (see green lines in Fig. 6) have considerable fluctuations for different distances. Fig. 7 shows the distribution of EVM estimation error using a violin plot, where each violin shape represents 150 test samples. Compared with LR2, LR3 models, one can see that LR1 has a more concentrated estimation error distribution around the median error, i.e., 0. Besides, a similar estimation performance is observed between the LR1 and the FFNN models.

Table I shows the complexity of different EVM estimation schemes in terms of computational complexity and time consumption. We use floating-point operations (FLOPs) to

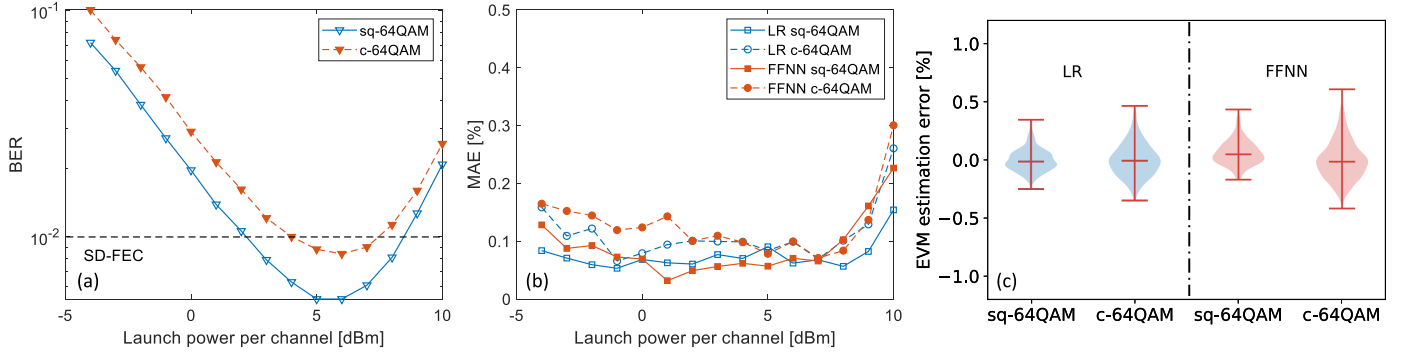


Fig. 9. (a) The BER versus launch power per channel curves. The EVM estimation performance on the test dataset: (b) the MAE versus launch power per channel, (c) the estimated EVM errors deviation.

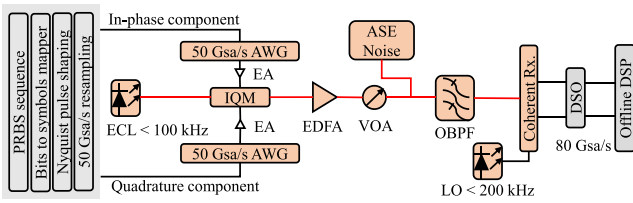


Fig. 10. 28 Gbaud experimental setup: EA: Electrical amplifier; VOA: Variable optical attenuator; DSO: Digital sampling oscilloscope.

TABLE I  
THE COMPLEXITY OF DIFFERENT EVM ESTIMATION SCHEMES  
ON A 64-BINS DATASET

| EVM Scheme    | FLOPs  | Training time [s] | Test time [s] |
|---------------|--------|-------------------|---------------|
| FFNN          | 1.73e6 | 32.4              | 3.0e-04       |
| LR            | 127    | 0.05 <sup>a</sup> | 8.5e-07       |
| Reference MFI | 402    | 1.7               | 9.8e-05       |

<sup>a</sup>The training time for a single modulation format.

measure the amount computation of the EVM model. For different devices, the time consumption may vary. This study uses a device with a 2.4 GHz Intel Xeon E5-2630-v3 with 64 GB of RAM and a GTX TITAN Black GPU. The FLOPs and test time are evaluated on a single 64-bin AH vector. For the LR-based scheme, we also provide a reference for the computational complexity and time consumption of an MFI module. The MFI is designed to identify the considered three modulation formats from a 64-bin AH vector. The employed neural network is an FFNN containing a 64-neuron input layer, a 5-neuron hidden layer and a 3-neuron output layer. It can be observed that the LR-based EVM estimation scheme has lower computational complexity and time consumption when the MFI module is also included. To benchmark, the computational complexity of the conventional EVM scheme [13], [14] is  $3n+3$  additions and  $2n+5$  multiplications, where  $n$  is the number of symbols. Taking 6400 symbols as an example it needs 19203 additions and 12805 multiplications, and the associated time of EVM estimation takes  $3.57e-2$  s [19], which is over two orders of magnitude longer than the LR approach as shown in Table I.

Besides, the conventional EVM calculation is implemented after the CPR. Thus, the process of CPR is also contributed to a degree of complexity. This part of complexity may vary for different system implementations; and the detailed analyses are reported in [27]–[29].

### C. Wavelength-Division Multiplexed Transmission

After studying long-haul transmission scenarios, we further investigate the generalization capability of the LR scheme for WDM transmission. Such transmission links might be impacted by intra- and inter-channel fiber nonlinearities. Fig. 8 shows a 32 GBaud 5-channel WDM system with 200-km long SSMF transmission using the 50 GHz ITU grid. The center channel is under test. We choose sq-64QAM and c-64QAM (as an example of a geometrically shaped constellation) modulation formats for this study. Fig. 9(a) shows the BER curves while we sweep the launch power (per channel) from  $-4$  dBm to  $+10$  dBm; note that the optical launch power for this configuration is 6 dBm per channel. It can be observed that both square and circular 64QAM achieves the BER below the SD-FEC after 200 km transmission. Thus, the fiber nonlinearity effects can be separately studied without features dominated by additive noises. For the LR scheme, we train each modulation format separately, whereas we mix them when training for the FFNN scheme so that we can use it as a reference. Fig. 9(b) and (c) show the EVM estimation performance on the test dataset. One can observe that the estimated EVM MAE of both the FFNN and the LR models are slightly affected by nonlinearities. This indicates that the phase distortion of some cases in the nonlinear noise-limited region is barely transferred to the AH. In this case, the deviations between the estimated EVM values and the true EVM values on the test samples are within 0.5%, which shows a good EVM estimation capability.

## IV. EXPERIMENTAL VALIDATION AND RESULTS

We carry out an experimental validation for 28 Gbaud sq-64QAM and c-64QAM signals, the setup is shown in Fig. 10. At the transmitter side, a PRBS15 is generated, and Gray mapped

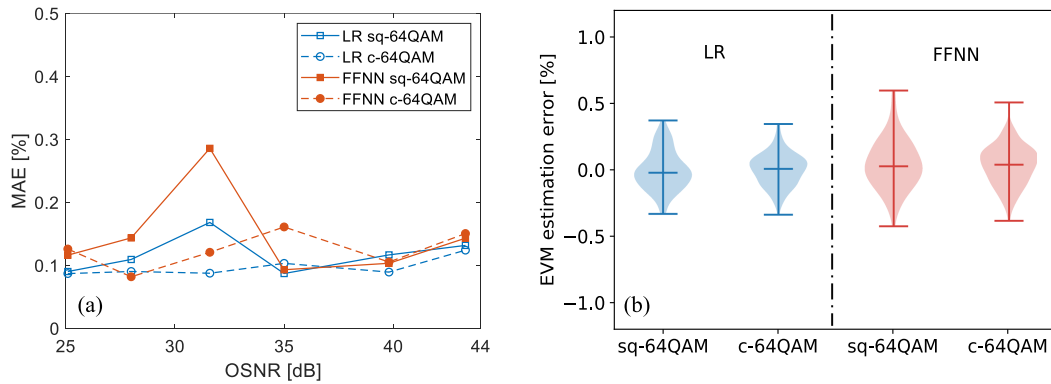


Fig. 11. The EVM estimation performance on the test dataset: (a) MAE vs. OSNR (b) Estimated EVM errors deviation.

onto complex symbols corresponding to two modulation formats, i.e., sq-64QAM and c-64QAM. Then, the 28 Gbaud signals are generated by filtering the complex symbols with the Nyquist pulse shaper of 0.15 roll-off factor and resampled to 50 GSa/s, before being loaded to two synchronized arbitrary waveform generators (AWG, Tektronix AWG70001A, 50 GSa/s). After that, the in-phase and quadrature electrical signals at the outputs of the AWGs are amplified by a pair of linear electrical amplifiers (EAs, SHF 827). The IQM with a 3-dB bandwidth of 25 GHz modulates the incoming electrical signals onto a continuous wave (CW) optical carrier launched by an external cavity laser (ECL, 1550.2 nm, 10-dBm) of  $\sim 100$  kHz linewidth to obtain the modulated optical signals. A booster EDFA is used to compensate the modulation loss of the IQM and keep the transmitted signal power constantly at 5 dBm. The OSNR adjusting module consists of a variable optical attenuator (VOA) and an amplified spontaneous emission (ASE) noise source. After the noise loading, the signal is received by a coherent receiver. The receiver contains a balanced coherent receiver front end, a 200 kHz local oscillator (LO) laser, and a real-time digital storage oscilloscope (DSO, Keysight DSOX93304Q, 80 GSa/s, 33 GHz). We set 6 OSNR values ranging from 25 dB to 44 dB for each modulation format and save the corresponding signal waveforms for further dataset accumulation. For each transmission scenario, we collect 100 AHs before the CPR in the offline digital signal processing (DSP). Each AH has 64 amplitude bins represented by 6400 symbols. The true EVM label of each transmission scenario is calculated after the full DSP routine. We use 50%, 25%, 25% of the dataset for training, validation, and testing, respectively.

The EVM estimation results during the testing process are shown in Fig. 11. As previously discussed, we train the LR-based EVM estimator for each modulation format separately. Whereas the reference FFNN-based model is trained by all modulation formats together. The MAE as a function of OSNR is shown in Fig. 11(a), the LR model achieves an MAE below 0.2%. In addition, the estimated EVM deviations for LR scheme are within 0.5% (Fig. 11(b)). Consistent with previous simulation results, the separately trained LR-based EVM estimation model can achieve comparable performance as an FFNN model. This implies that a simple LR-based EVM estimation model can be compensated for the lack of

nonlinearity functions by pre-classification of modulation formats. It is noticed that in our simulation and experiment we use signals in single-polarization to keep consistency. However, since the approach/conclusions are general, they can be extended to a dual-polarization configuration.

## V. CONCLUSION

In this work, we investigate the application of a simple LR-enabled EVM estimator for signal quality monitoring in coherent optical systems. This scheme can estimate EVM from the AH of a signal sequence captured before CPR. Since the LR model is a simplified FFNN without hidden layers and nonlinear activation functions, the estimation capability of the LR model is limited. Thus, we train the LR model for each modulation format separately to maximize inference capability. Normally, the modulation format information can be obtained by an MFI module of OPM. Then, a trained modulation-format-wise EVM estimation model can be selected to perform fast and robust signal quality monitoring. The simulation and experiment have demonstrated feasibility and versatility of the LR-based EVM estimator, which achieves comparable performance as the FFNN-based model. We believe that the simple LR-based EVM estimator has the potential to be applied in the OPM module to extend the monitoring functionality and ensure robust networking operation.

## REFERENCES

- [1] K. Roberts, Q. Zhuge, I. Monga, S. Gareau, and C. Laperle, "Beyond 100 Gb/s: Capacity, flexibility, and network optimization," *J. Opt. Commun. Netw.*, vol. 9, pp. C12–C23, 2017.
- [2] O. Gerstel, M. Jinno, A. Lord, and S. J. B. Yoo, "Elastic optical networking: A new dawn for the optical layer?," *IEEE Commun. Mag.*, vol. 50, no. 2, pp. s12–s20, Feb. 2012.
- [3] H. Lun et al., "Machine-learning-based telemetry for monitoring long-haul optical transmission impairments: Methodologies and challenges," *J. Opt. Commun. Netw.*, vol. 13, pp. E94–E108, 2021.
- [4] Rui Manuel Morais, "On the suitability, requisites, and challenges of machine learning," *J. Opt. Commun. Netw.*, vol. 13, pp. A1–A12, 2021.
- [5] D. C. Kilper et al., "Optical performance monitoring," *J. Lightw. Technol.*, vol. 22, pp. 294–304, 2004.
- [6] C. Yu, H. Wang, C. Ke, Z. Liang, S. Cui, and D. Liu, "Multi-task learning convolutional neural network and optical spectrums enabled optical performance monitoring," *IEEE Photon. J.*, vol. 14, no. 2, Apr. 2022, Art. no. 7217808.

- [7] D. Wang et al., "Optical performance monitoring of multiple parameters in future optical networks," *J. Lightw. Technol.*, vol. 39, pp. 3792–3800, 2021.
- [8] M. Ruiz, D. Sequeira, and L. Velasco, "Deep learning-based real-time analysis of lightpath optical constellations," *J. Opt. Commun. Netw.*, vol. 14, pp. C70–C81, 2022.
- [9] F. N. Hauske, M. Kuschnerov, B. Spinnler, and B. Lankl, "Optical performance monitoring in digital coherent receivers," *J. Lightw. Technol.*, vol. 27, pp. 3623–3631, 2009.
- [10] J. Chai, X. Chen, Y. Zhao, T. Yang, D. Wang, and S. Shi, "Joint symbol rate-modulation format identification and OSNR estimation using random forest based ensemble learning for intermediate nodes," *IEEE Photon. J.*, vol. 13, no. 6, Dec. 2021, Art. no. 7900106.
- [11] B. Szafraniec, T. S. Marshall, and B. Nebendahl, "Performance monitoring and measurement techniques for coherent optical systems," *J. Lightw. Technol.*, vol. 31, no. 4, pp. 648–663, 2013.
- [12] F. N. Khan, Z. Dong, C. Lu, and A. P. T. Lau, "Optical performance monitoring for fiber-optic communication networks," in *Enabling Technologies for High Spectral-Efficiency Coherent Optical Communication Networks*. Hoboken, NJ, USA: Wiley, 2016.
- [13] R. Schmogrow et al., "Error vector magnitude as a performance measure for advanced modulation," *IEEE Photon. Technol. Lett.*, vol. 24, no. 1, pp. 61–63, Jan. 2012.
- [14] I. Fatadin, "Estimation of BER from error vector magnitude for optical coherent systems," *Photonics*, vol. 3, no. 2, pp. 21–26, Apr. 2016.
- [15] C. Zhu et al., "Statistical moments-based OSNR monitoring for coherent optical systems," *Opt. Exp.*, vol. 20, pp. 17711–17721, 2012.
- [16] X. Lin, O. A. Dobre, T. M. N. Ngatched, and C. Li, "A non-data-aided OSNR estimation algorithm for coherent optical fiber communication systems employing multilevel constellations," *J. Lightw. Technol.*, vol. 37, no. 15, pp. 3815–3825, Aug. 2019.
- [17] D. Wang et al., "Intelligent constellation diagram analyzer using convolutional neural network-based deep learning," *Opt. Exp.*, vol. 25, pp. 17150–17166, 2017.
- [18] C. Peng et al., "Long short-term memory neural network for mitigating transmission impairments of 160 Gbit/s PAM4 microring modulation," in *Proc. Opt. Fiber Commun. Conf.*, 2021, pp. 1–3.
- [19] Y. Fan et al., "Fast signal quality monitoring for coherent communications enabled by CNN-based EVM estimation," *J. Opt. Commun. Netw.*, vol. 13, pp. B12–B20, 2021.
- [20] Y. Fan et al., "Experimental validation of CNNs versus FFNNs for time- and energy-efficient EVM estimation in coherent optical systems," *J. Opt. Commun. Netw.*, vol. 13, pp. E63–E71, 2021.
- [21] Y. Fan et al., "Laser linewidth tolerant EVM estimation approach for intelligent signal quality monitoring relying on feedforward neural networks," in *Proc. Eur. Conf. Exhib. Opt. Commun.*, 2021, pp. 1–4.
- [22] S. Jiao, Y. Gao, J. Feng, T. Lei, and X. Yuan, "Does deep learning always outperform simple linear regression in optical imaging?," *Opt. Exp.*, vol. 28, pp. 3717–3731, 2020.
- [23] Y. Fan et al., "EVM estimation for performance monitoring in coherent optical systems: An approach of linear regression," in *Proc. Conf. Lasers Electro-Opt.*, 2022, pp. 1–12.
- [24] K. Hornik, M. Stinchcombe, and H. White, "Multilayer feedforward networks are universal approximators," *Neural Netw.*, vol. 2, no. 5, pp. 359–366, 1989.
- [25] VPIphotonics GmbH, "VPItransmissionMaker11," 2021. Accessed: Oct. 13, 2021. [Online]. Available: <https://www.vpiphotonics.com/>
- [26] D. A. Freedman, *Statistical Models: Theory and Practice*. Cambridge, U.K.: Cambridge Univ. Press, 2009.
- [27] J. R. Navarro et al., "Carrier phase recovery algorithms for coherent optical circular mQAM systems," *J. Lightw. Technol.*, vol. 34, no. 11, pp. 2717–2723, Jun. 2016.
- [28] P. Zhang et al., "Low-complexity blind carrier phase recovery for C-mQAM coherent systems," *IEEE Photon. J.*, vol. 11, no. 1, Feb. 2019, Art. no. 7200214.
- [29] J. C. M. Diniz et al., "Low-complexity carrier phase recovery based on principal component analysis for square-QAM modulation formats," *Opt. Exp.*, vol. 27, pp. 15617–15626, 2019.